Mechanical and Functional Properties of Laser-Welded Ti-55.8 Wt Pct Ni Nitinol Wires

B. TAM, M.I. KHAN, and Y. ZHOU

As interest increases in incorporating Nitinol alloys in different microapplications and devices, the development of effective procedures for laser microwelding (LMW) these alloys becomes necessary. Laser welding processes applied to Nitinol have been shown to lower strength, induce inclusions of intermetallic compounds (IMCs), and alter the pseudoelastic and shape memory effects. Inconsistency in reported weld properties has also suggested that further studies are required. The current study details the mechanical, microstructural, and phase transformation properties of Nd:YAG LMW crossed Ti-55.8 wt pct Ni Nitinol wires. The effects of surface oxide on joint performance were also investigated. Fracture strength, weld microstructure, and phase transformation temperatures at varying peak power inputs were studied and compared to the unaffected base metal. Results showed good retention of strength and pseudoelastic properties, while the fusion zone exhibited higher phase transformation temperatures, which altered the active functional properties at room temperature.

DOI: 10.1007/s11661-011-0639-6

I. INTRODUCTION

NITINOL shape memory alloys are widely used in medical, aerospace, and micro-electrical-mechanical systems applications.[1] Primary fabrication processes in these applications include laser cutting and special hot/cold shaping techniques.[1–3] As demands increase for finer and more complex devices, advancement in effective processing methods becomes necessary, including welding and joining methods. Pulsed Nd:YAG laser microwelding (LMW) is an ideal joining process for micro- and macrodevices, since its high energy density can create miniature joints with a small heat-affected zone (HAZ).[4] However, LMW of Nitinol is considered difficult, since its inherent functional properties (pseudoelasticity and shape memory effect) are susceptible to change when exposed to high-temperature thermal cycles or chemical contamination, which is commonly encountered during laser welding.[5] Hence, it is essential to understand the cause and effects of these modifications to the overall performance of the joined components.

To date, limited studies exist in detailing the mechanical properties of Nd:YAG laser-welded Nitinol. After laser welding, Nitinol generally exhibits good retention of base material strength;[3,6,7] however, conflicting results have been reported regarding the pseudoelastic properties and fracture mechanism. For example, Schlossmacher *et al.* investigated laser welding of Nitinol sheets and observed no deterioration in pseudoelasticity and a ductile fracture mechanism.[6] In contrast, a study on laser-welded wires conducted by Yan *et al.* reported a lower critical stress for stress-induced martensite (SIM) transformation and an increased residual strain upon unloading.[2,3] The aforementioned study and another conducted by Ogata *et al.*[7] reported brittle fracture surfaces after tensile failure, contrary to what was observed by Schlossmacher *et al.*[6]

The functional properties (pseudoelasticity and shape memory effect) of Nitinol are strongly linked to its ability to phase transform between martensite and austenite and have been shown to change after being subjected to laser welding processes. An earlier study by Hsu *et al.* observed a slight decrease in transformation temperature after laser welding.[8] Similarly, Ogata *et al.*[7] and Tussi *et al.*[9] also reported a minimal effect on transformation temperatures. In a later study, Yan *et al.* observed a decrease in pseudoelastic properties and suggested this was caused by a decrease in transformation temperatures.[3] Attempts to explain these changes were made by Falvo *et al.*[10] and Song *et al.*,[11] both of which stated that laser welding modified base material similarly to solution treatment, removing the effect of previous thermomechanical processing. More recently, Khan and Zhou confirmed the effects of laser melting on transformation temperature, which was altered by more than 100 K, and characterized the effects using detailed thermal and metallurgical analyses.[12] It was shown that laser-processed Nitinol had distinct changes in microstructural and mechanical properties as compared to the base metal. The authors suggested that preferential vaporization of nickel played a role in the change in local transformation temperature. Overall, these recent developments suggest that additional detailed analysis is required to understand the

B. TAM, MASc Student, M.I. KHAN, PhD Student, and Y. ZHOU, Professor, are with the Micro-Welding Laboratory, Centre for Advanced Materials Joining, Department of Mechanical Engineering, University of Waterloo, Waterloo, ON, Canada L5C-3M8. Contact e-mail: Ibraheem@rogers.com

Manuscript submitted June 10, 2010.
Article published online March 15, 2011

modifications to mechanical and transformation behaviors of welds. These effects must be thoroughly understood in order to refine protocols to achieve functional weldments. Hence, the objective of the current study is to evaluate the effect of peak power inputs during pulsed Nd:YAG laser welding on the mechanical, metallurgical, and phase transformation behaviors of welded Nitinol wires.

II. EXPERIMENTAL SETUP

A. *Laser Welding*

Commercially available, 0.410-mm-diameter, pseudoelastic Nitinol wires were used in this study. Wires were Ni rich at Ti-55.8 wt pct Ni with maximum carbon and oxygen contents of 0.05 wt pct. Previous thermomechanical processing was performed by the manufacturer to optimize the mechanical properties for medical device applications. Prior to welding, a dilute solution of hydrofluoric and nitric acid was used to remove surface oxide and contaminants. The rate of metal dissolution was examined using six different treatment times: 5, 10, 20, 30, 40, and 50 seconds. A treatment time of 20 seconds was used for wires to be welded for mechanical testing and microstructural examinations.

Laser welding was performed using a pulsed Nd:YAG laser having a wavelength of 1064 nm. The beam had a nominal spot diameter of 400 μm with a Gaussian power distribution. Peak power was varied between 0.55 and 1.75 kW. Welds were produced using a trapezoidal pulse schedule, with a weld time of 5 and 1 ms up and down slopes. Argon shielding at a feed rate of 30 CFH was maintained throughout the welding time to minimize oxidation, in accordance with a previous study on titanium alloys.[13] The beam was focused centered at the intercept of the crossed wires using a positioning laser. A downward force was applied using a special fixture that elastically deformed the wires onto a single plane, illustrated in Figure 1.

B. *Mechanical Testing and Microstructural Analysis*

Joint strength was expressed as the joint breaking force (JBF) determined by an Instron* 5548 microtensile tester.

*INSTRON is a trademark of Instron, Canton, MA.

The crosshead speed was set to 0.4 mm/min, and the tensile-shear test direction is shown in Figure 2. A minimum of five samples were tested for each welding condition. Fracture surfaces were examined using scanning electron microscopy (SEM). Micro-Vickers hardness was measured using a Shimadzu microhardness tester (Shimadzu Corporation, Kyoto, Japan). A series of 50 g indents, 40 μm apart, held for 20 seconds were made along the longitudinal centerline of the welds. Samples were etched with a 14 mL HNO3, 3 mL HF, and 82 mL H2O solution for 25 to 30 seconds. The microstructure was observed using optical microscopy and SEM.

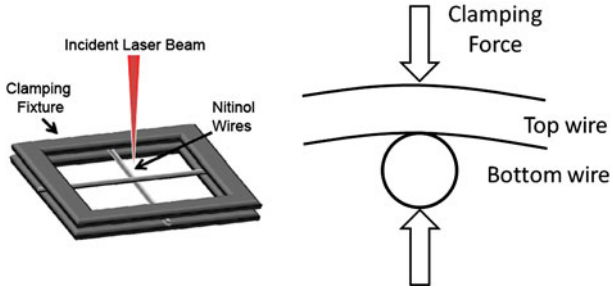

Fig. 1—Schematic of sample fixturing.

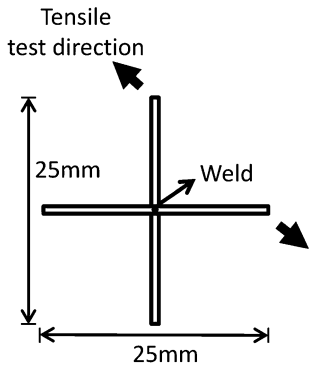

Fig. 2—Schematic of tensile test.

C. *Phase Analysis*

Phase transformation temperatures were measured by differential scanning calorimetry (DSC) using a thermal analysis Q2000 system equipped (TA Instruments, New Castle, DE) with a refrigerated cooling system. Tests were conducted between 198 K and 373 K (–75 °C and 100 °C), controlled at a rate of 5 °C per minute. Onset temperatures for phase transformations were determined as the intersection of tangents to the slope of a peak with the base line. Welded samples were carefully sheared off from the base metal material; however, due to the small scale, some remnant base metal material remained on the DSC samples. Base metal, quenched in water from 1 hour of heating at 1073 K (800 °C) to attain solid-solution condition, was also tested to observe its intrinsic phase transformation behavior. X-ray diffraction (XRD) analysis on fusion zones was performed using metallographic samples to determine the crystal structure. XRD scans were conducted with a 0.3-mm collimator on a Rigaku MSC micro-XRD (Rigaku Corporation, Tokyo, Japan) that uses Cu K_α X-rays of 1.54 A wavelength.

III. RESULTS AND DISCUSSION

A. *Effects of Oxide Removal*

Nitinol's affinity to form a tenacious oxide layer can potentially create weld defects.[15–17] Hence, the as-received wires were immersed in an acid solution to remove surface oxide and contaminants. Since prolonged acid immersion can excessively reduce the wires' cross-sectional diameter, a preliminary study was con-

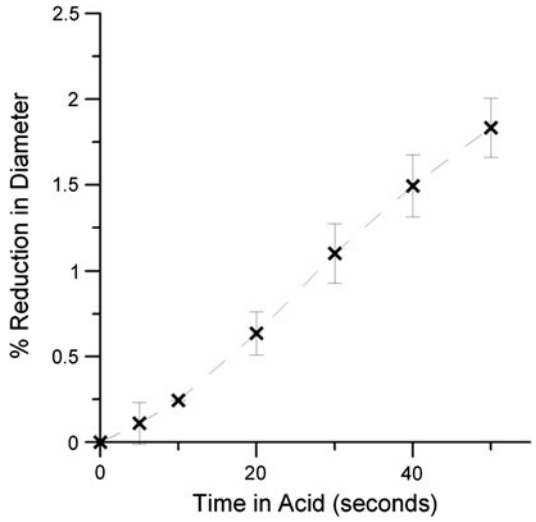

Fig. 3—Effect of time in acid on percent reduction in diameter.

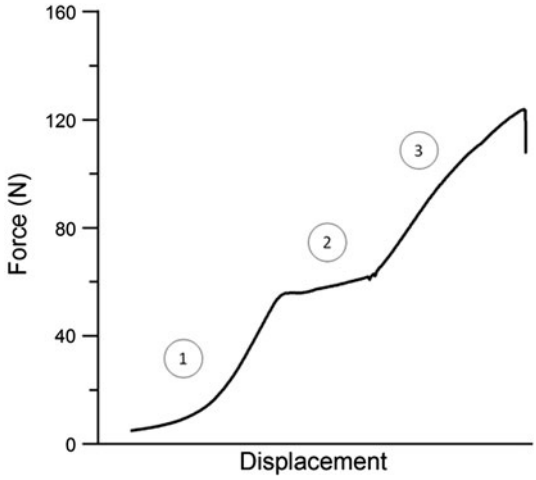

Fig. 5—Force and displacement curve using 1.0 kW peak power: (1) elastic response of austenite, (2) SIM, and (3) elastic/plastic deformation of martensite.

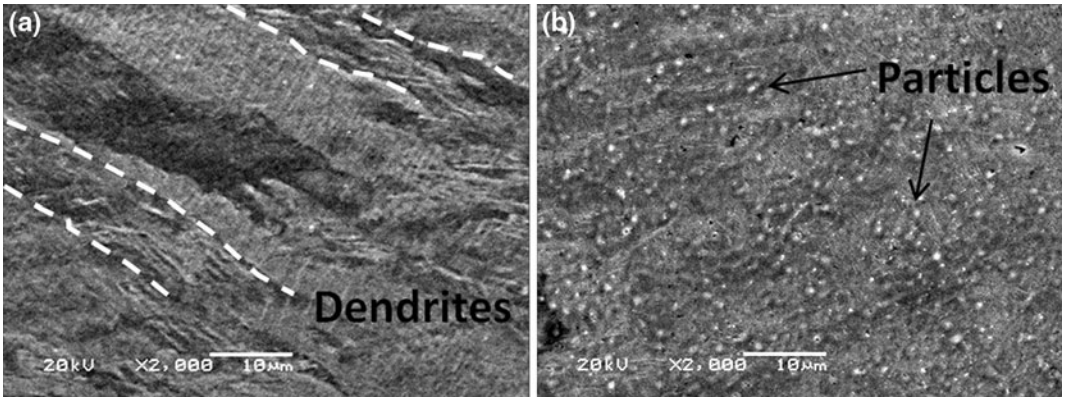

Fig. 4—Fusion zones of welds (*a*) with and (*b*) without surface cleaning by acid solution.

ducted to analyze these effects and select an appropriate treatment time. Figure 3 shows the percent reduction in diameter, which was linearly proportional to treatment time. Residual surface oxides remained visible at short treatment time. Immersion time of 20 seconds was selected for the current study, since there was minimal residual oxide remaining at the surface, while diameter reduction was less than 1 pct.

A substantial increase in weld strength was also observed when acid treating wires prior to welding. Although the welds could not be differentiated visually in surface appearance, cross-sectional SEM profiles (Figure 4) revealed distinct microstructures in the fusion zone. The dendritic structure typically observed in fusion welds was observed in the cleaned wire, whereas the untreated wire contained particles and no clear dendritic structure. Particles in the untreated wire are believed to be finely dispersed Ti-Ni-O intermetallics that can act as nucleation sites during solidification, altering the solidification structure.[14,15] Similar observations were reported during the production of Nitinol ingots.[16] In general, inclusions of carbon and oxygen are kept to a minimum, because Ti-Ni-O intermetallic compounds (IMCs) have lattice structure of large misfits with Nitinol, creating incoherent precipitates that can cause premature failure.[17]

B. *Mechanical Properties of Welded Joints*

Laser welding was found to effectively preserve pseudoelasticity, as shown by the load- displacement curve (Figure 5). Although test geometries make it difficult to attain the absolute stress-strain behavior, the distinct phases of pseudoelastic response were still exhibited. Each of these responses can be observed in Figure 5 including (1) elastic deformation of the austenitic phase, (2) SIM transformation, and (3) elastic and plastic deformation of martensite until failure.

The effect of peak power on the JBF of weld specimens is shown in Figure 6. A minimum peak power of 0.55 kW was required to produce joints. Near the onset of joining (0.5 to 0.7 kW), low JBFs were attained. Joint strength increased steadily beyond 0.7 kW, with maximum JBFs of 110 to 120 N achieved between 0.85 and 1.7 kW. The equivalent fracture stress (calculated based on the wire diameter) was comparable

to the literature, approximately 70 to 80 pct of base metal.[3,6,7] Peak powers exceeding 1.7 kW resulted in overwelding.

Trends in the JBF could be associated with the observed fracture surface. Figure 7 shows SEM micrographs of a weld using a peak power input of 0.6 kW, which had a low JBF of approximately 10 N. The visible/unmelted bottom wire in Figure 7(b) signified insufficient energy was provided by the incident beam at this condition. Lack of bonding resulted in a notch that served as a site for fracture initiation. This can be observed in Figure 7(d), where a nonbonded region was visible near the weld interface of the fracture surface. Failure then proceeded along the weld metal, characterized by a fine dimpled morphology (Figure 8(b)) that correlated to the fine dendritic structure produced from rapid solidification. In contrast, base metal failure exhibited a ductile morphology of larger dimples (Figure 8(a)).

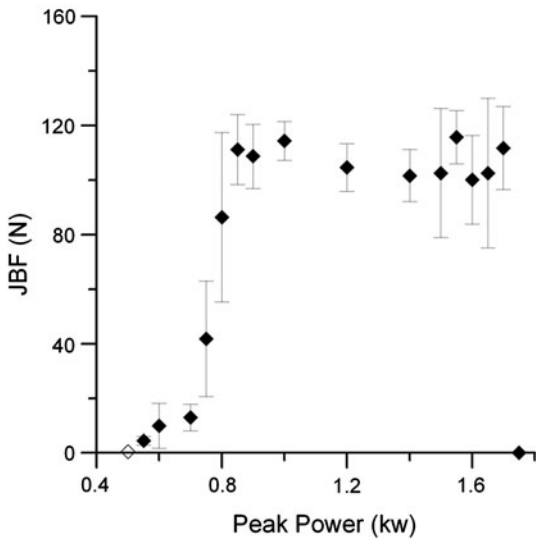

Fig. 6—JBF using different peak powers.

Full penetration was observed when peak powers above 0.8 kW were applied (Figure 9), which was accompanied with a substantial improvement in strength (from 10 to 80 N). A fusion-zone gradient was clearly visible, with melting at the bottom surface not as pronounced as on the top side (Figure 9(b)). When compared to the 0.6 kW weld, the failure path transitioned from one wire to through the fusion zone of both wires (Figures 9(c) and (d)).

Smoother joint surfaces were achieved when using conditions producing maximum JBF values (0.85 to 1.7 kW) (Figures 10 and 11). In addition to eliminating potential stress risers, smooth surfaces are essential to *in-vivo* medical devices for minimizing damage to organs and tissues during implantation and operation.[18] Fracture in these joints proceeded along the base and weld metals at the lower power range (regions are traced out in Figure 10(d)) to only weld metal at the upper power range (Figure 11(c)). Joints were more susceptible to undercutting at high peak power inputs (Figure 11(a)), which reduces local load bearing capacity. This was

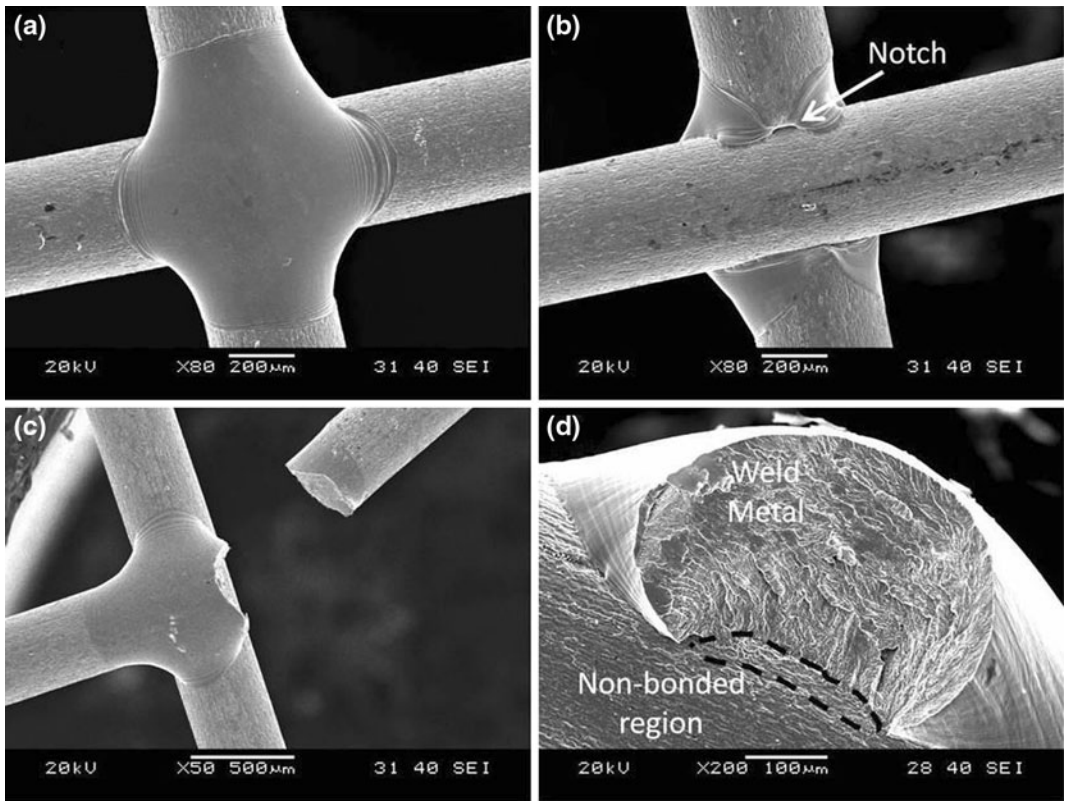

Fig. 7—SEM images of welds made at 0.6 kW peak power for the (*a*) weld top, (*b*) weld bottom, (*c*) fractured weld, and (*d*) fracture surface.

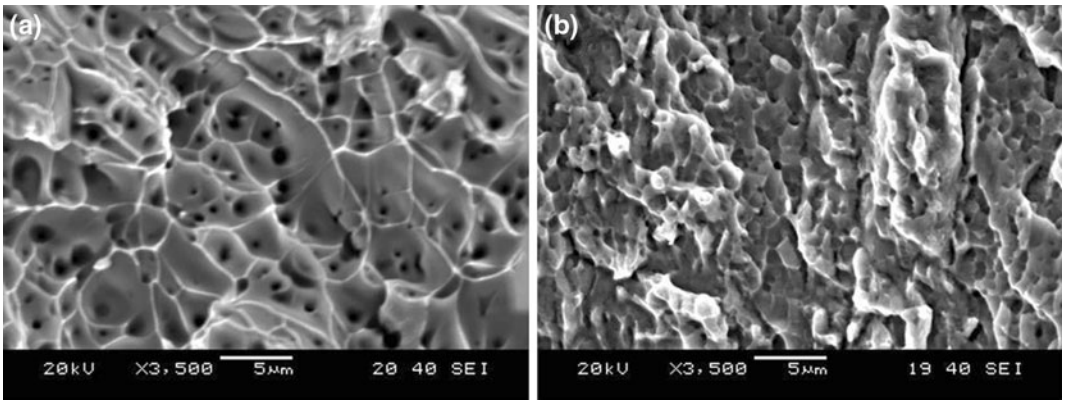

Fig. 8—High-magnification SEM fracture surfaces of (*a*) base and (*b*) weld metals.

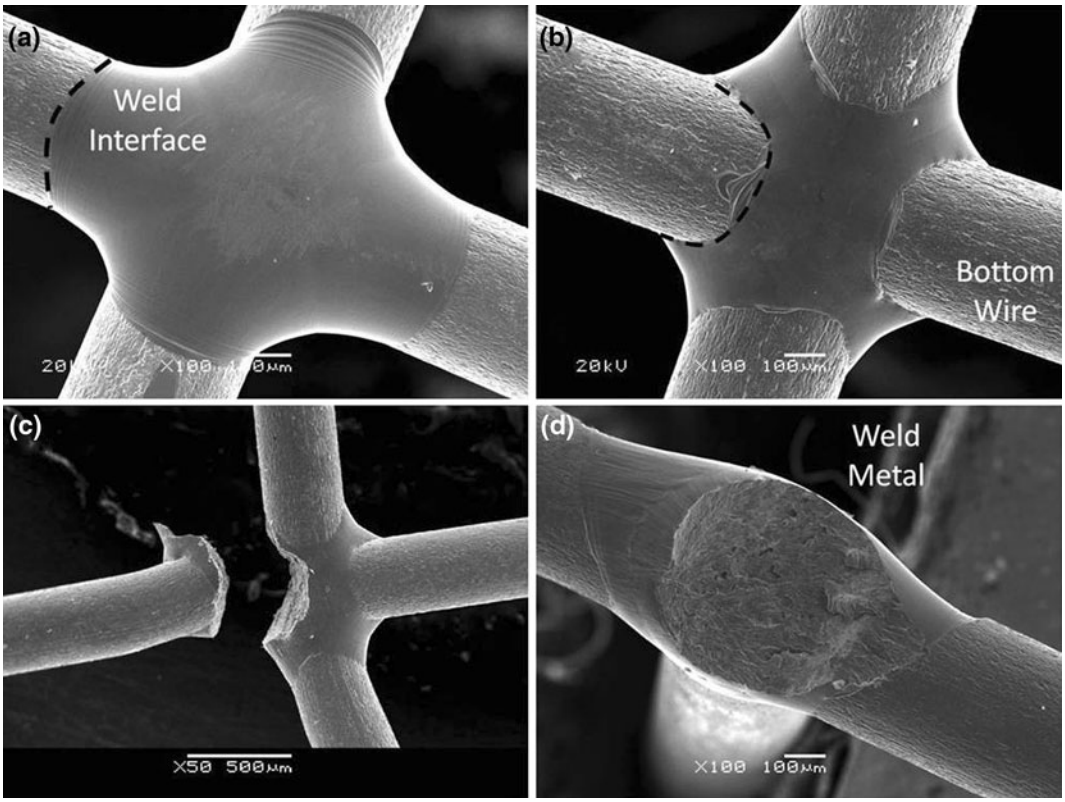

Fig. 9—SEM images of welds made at 0.8 kW peak power for the (*a*) weld top, (*b*) weld bottom, (*c*) fractured weld, and (*d*) fracture surface.

reflected in the higher standard deviation of strength at high powers in Figure 6. Finally, overwelding was observed when peak powers of 1.75 kW or higher were applied (Figure 12).

C. *Microstructure and Hardness*

A cross-sectioned joint made at 0.6 kW is shown in Figure 13. Base metal consisted of a fine-grained unidirectional structure produced during the cold drawing process. The upper wire was the first exposed to laser irradiation with local peak temperatures surpassing the alloy's liquidus temperature. Termination of laser power resulted in rapid cooling and solidification of the molten metal, forming the columnar dendritic structure. The bottom wire was partly melted, as shown by the recrystallized microstructure in site A (Figure 13(b)). Lack of bonding was observed at the peripheral junction of the two wires, detailed in site B (Figure 13(c)).

Cross-sectioned views of a weld produced at 1.0 kW showed weld widths at the top and bottom to be more equal, as observed in Figure 14(a). Upon closer examination near the fusion boundary, site A shown in Figure 14(b), the recrystallized HAZ was observed beside the fine-grained unaffected base material. Near the fusion boundary, a region of small columnar grains

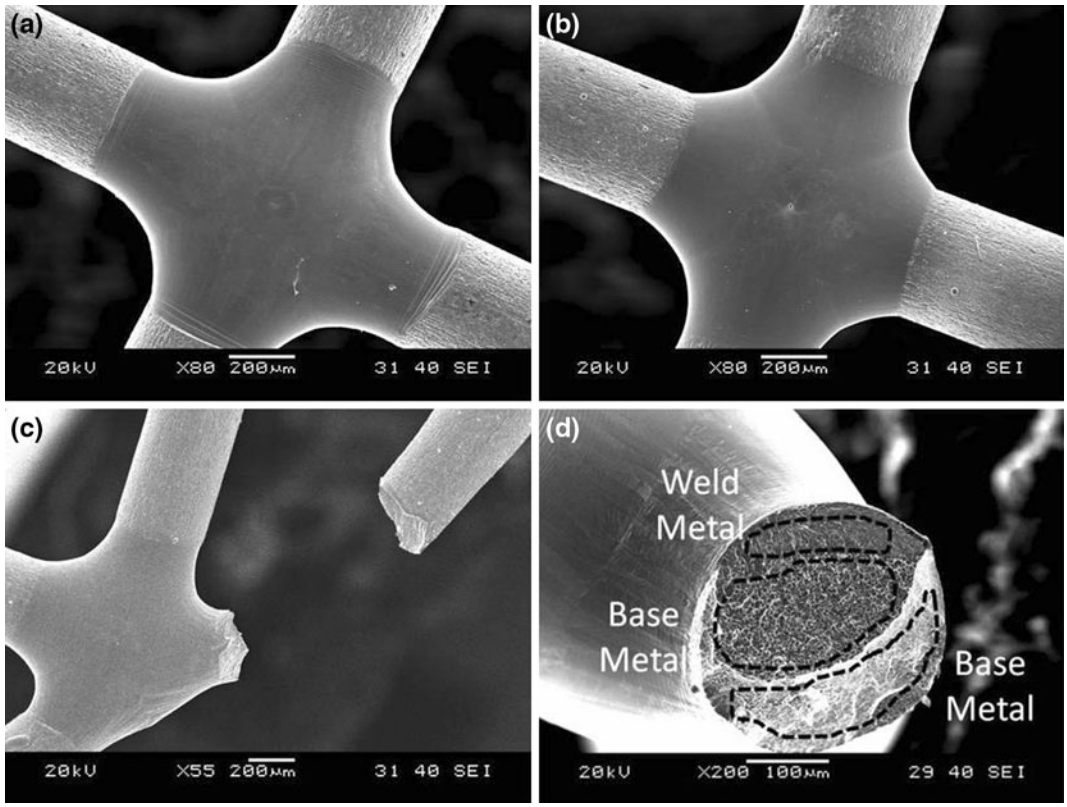

Fig. 10—SEM images of welds made at 1.0 kW peak power for the (*a*) weld top, (*b*) weld bottom, (*c*) fractured weld, and (*d*) fracture surface.

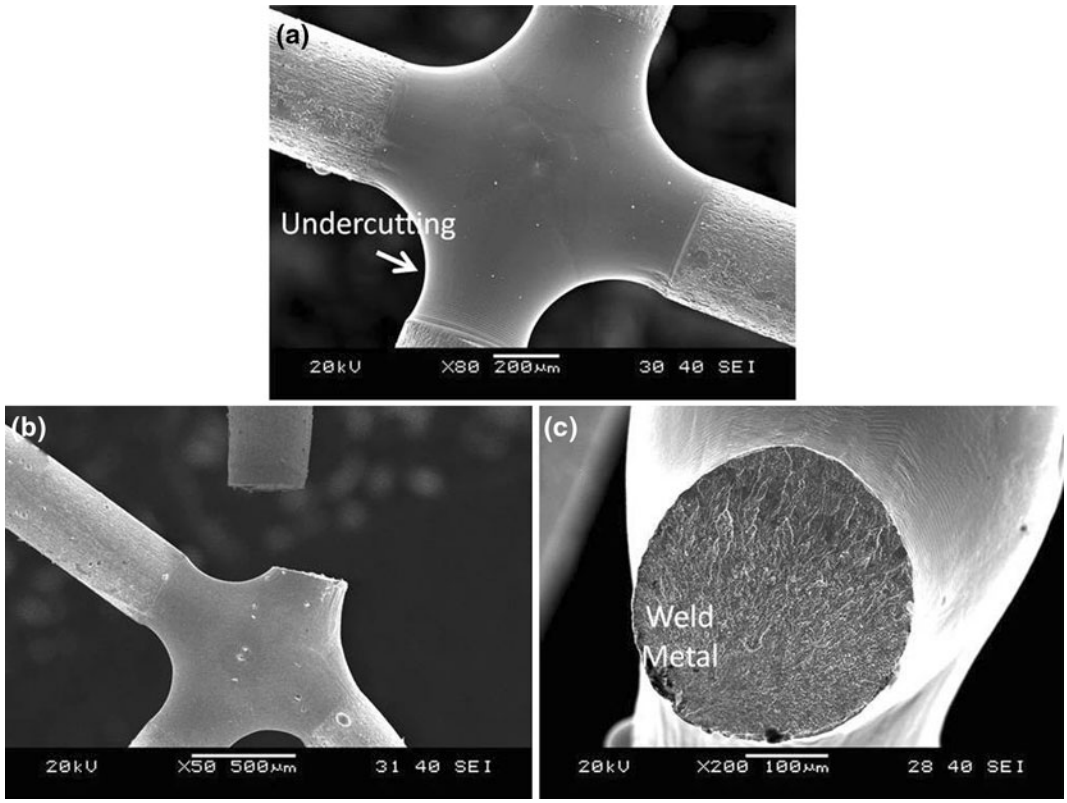

Fig. 11—SEM images of welds made at 1.6 kW peak power for the (*a*) weld top, (*b*) weld bottom, and (*c*) fracture surface.

formed, likely due to competitive growth. The fusion zone consisted of larger columnar dendritic grains oriented normal to the centerline, suggesting the primary direction of heat withdrawal was conduction into the wires. Near the center, site B shown in Figure 14(c), dendrites that had grown perpendicular to the cross section were observed. A network of second-phase particles was also detected within the fusion zone; the particles were suspected to be $NiTi_2$ IMC, as observed in the referenced work, but their origin currently remains unclear.[2,6]

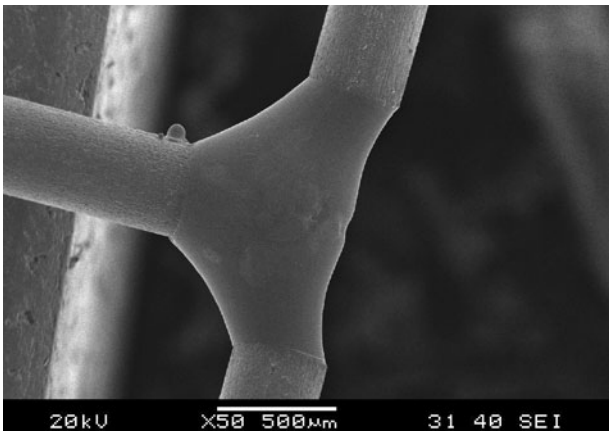

Fig. 12—SEM surface of a weld made at 1.75 kW peak power.

Further increasing peak power resulted in a wider fusion zone and HAZ with balanced melting at the top and bottom faces. This trend was clearly observed from the microhardness profiles for the 0.6, 1.0, and 1.6 kW welds, as shown in Figure 15. Base metal hardness was near 400 Hv and values decreased approaching the weld metal. The resolidification structure of the fusion zone experienced a 30 pct decrease to approximately 280 Hv. Heat conduction into the wire produced a gradient effect of recrystallization and grain growth of base metal. In turn, this resulted in a softening gradient due to the elimination of previous cold working. Increased fusion zone and HAZ sizes were observed with increasing peak powers, which is typically experienced with higher heat inputs during most welding processes.[19] However, the size of the local softened region was found to have minimal effects on JBFs as similar fracture strengths were attained between 0.85 and 1.7 kW.

Differences in weld and base metal properties generally can be related to the joining mechanism and the resulting softening. In previous studies on microresistance spot welding of Nitinol, resistance heating at the interface promoted solid-state bonding through grain growth.[5,18] Joint strength was shown to be a function of interfacial bond strength and HAZ softening due to

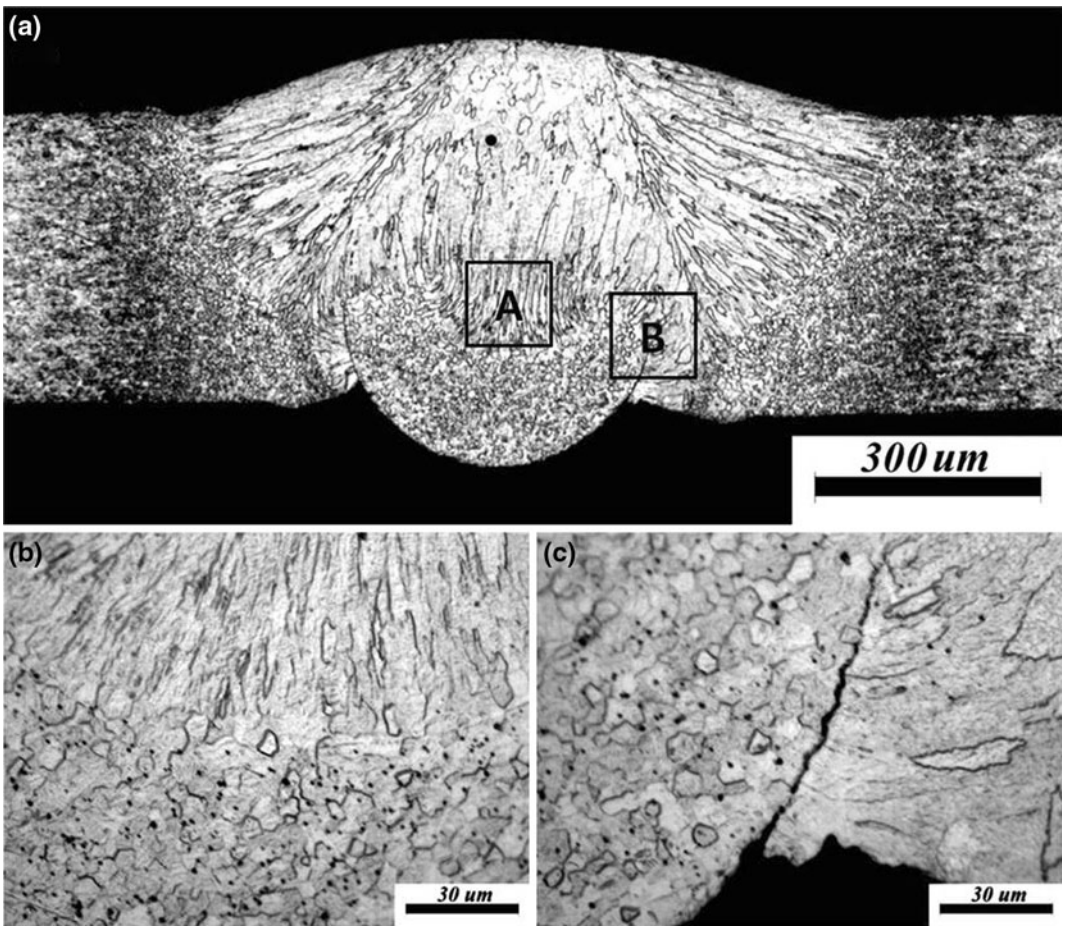

Fig. 13—Micrographs of welds made at 0.6 kW peak power showing the (*a*) overall cross section, (*b*) site A, and (*c*) site B.

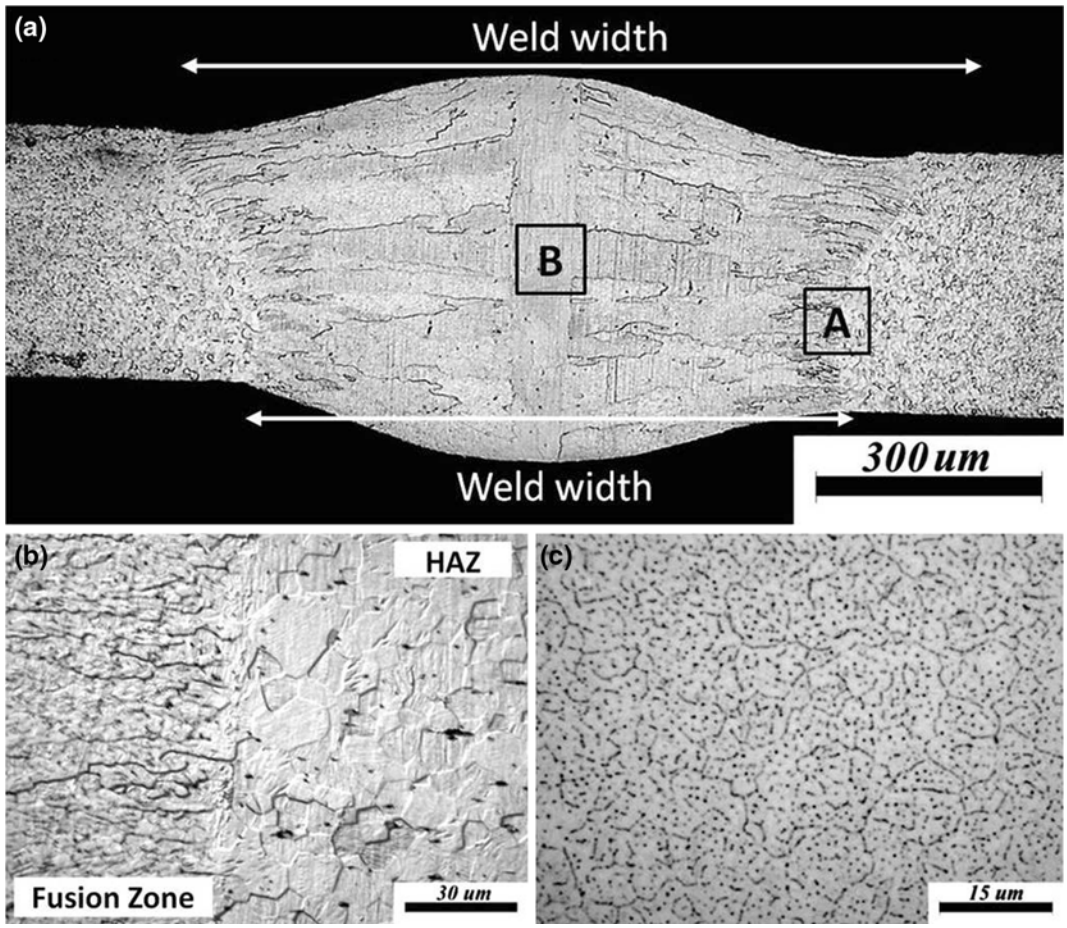

Fig. 14—Micrographs of welds made at 1.0 kW peak power showing the (*a*) overall cross section, (*b*) site A, and (*c*) site B.

grain recrystallization.[5] In contrast, joining in the current study was primarily fusion based with joint strength mainly depending on weld penetration and growth.

D. *Local Phase Transformation in Welded Joints*

DSC curves of base metal, fully annealed base metal, and select welds are shown in Figure 16 with respective onset temperatures summarized in Tables I and II. At room temperature, base metal primarily consisted of an austenitic structure. Broad temperature peaks of base metal, as a result of the preceding thermomechanical processing during wire fabrication, could no longer be observed after welding. In comparison, weld metals exhibited multiple transformations, including a pair of distinct high- and low-temperature peaks. These two distinct pairs of peaks could be associated with the different weld zones present in the sample, including the HAZ and fusion zone. The HAZ was responsible for the low-temperature peaks, which were similar to those of fully annealed wire. Heat conduction through the wires during welding removes the effects of prior cold working and heat treatments, similar to an annealing process. Hence, the low-temperature peaks were more prominent for the 0.6 kW sample because of the additional contribution of the recrystallized base metal of the bottom wire (Figure 13). In contrast, full penetration occurring at the higher power levels results in a smaller HAZ that is confined in the wire (Figure 14).

Distinct thermal peaks from the fusion zone at high temperatures, denoted by "FZ peaks" in Figure 16, suggest modification to the original crystal structure. Onset temperatures, martensite start (M_s) and austenite finish (A_f), of the fusion zones were in the range of 278 K to 286 K (5 °C to 13 °C) and 301 K to 311 K (28 °C to 38 °C), respectively, with a common transformational hysteresis of 293 K to 298 K (20 °C to 25 °C).[14] Modification to phase transformation temperatures varied with peak power inputs, showing that different welding parameters may have different effects on the transformation temperatures.

Room-temperature XRD analysis of the fusion zones confirmed the phase conversion induced by LMW of Nitinol. Two conditions were tested for the 1.0 kW weld, including heating above A_f and cooling to room temperature (condition 1) and cooling below M_s and heating to room temperature (condition 2). As expected from the DSC data, base-material-produced peaks corresponded to the B2 structure of austenite (Figure 17(a)). Similarly, condition 1 retained a homogeneous austenitic structure (Figure 17(b)). However,

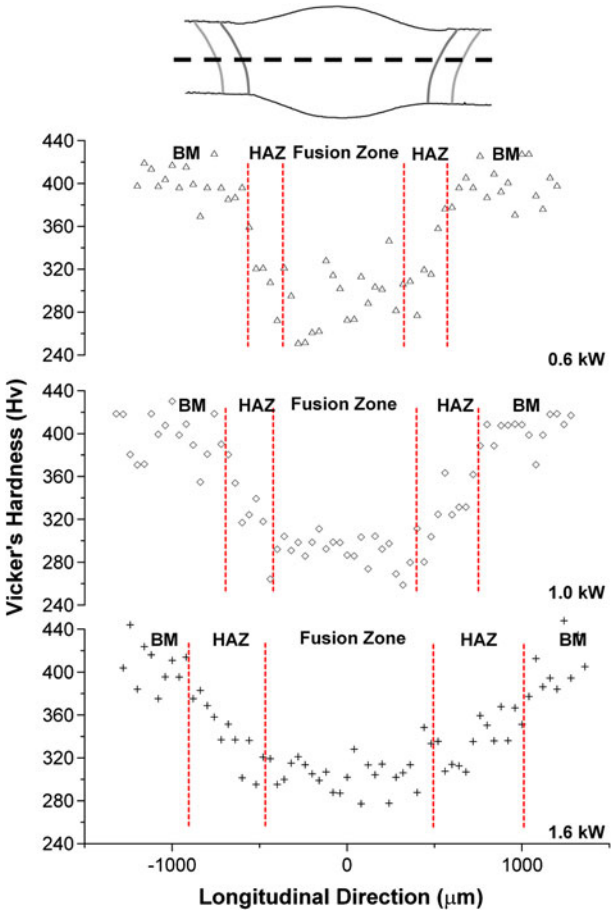

Fig. 15—Vickers hardness across the fusion zone of welds using peak powers of 0.6, 1.0, and 1.6 kW.

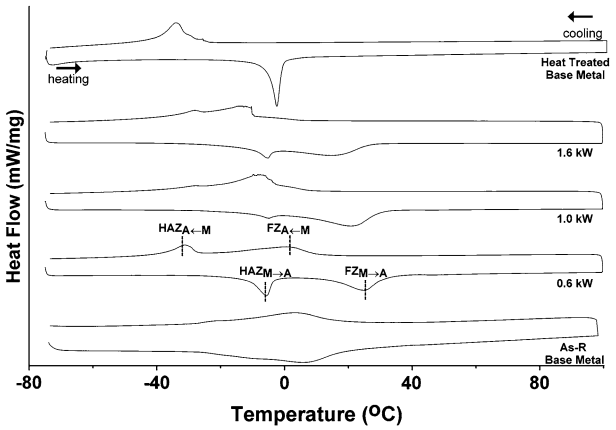

Fig. 16—DSC curves for as-received base metal, heat-treated base metal, and welds using peak powers of 0.6, 1.0, and 1.6 kW.

Table I. Temperature Onsets of Phase Transformations in Base Metal and Base Metal Treated at 1073 K (800 °C) for 1 H

Material Condition	M_s	A_f
As-received	19.14	19.65
Annealed	–28.66	–7.59

the coexistence of austenite and martensite at room temperature was detected for condition 2 (Figure 17(c)). This was due to the transformational hysteresis of the fusion zone, in which the structure can be thermally conditioned between A_s and A_f, resulting in an incomplete martensite-to-austenite transformation at room temperature.

The current result showed distinctly different transformation behavior in the weld metal as compared to the base metal. Phase transformation temperatures of the fusion zone increased with respect to base metal, which can be attributed to a combination of mechanisms. More specifically, the work done by Khan and Zhou suggests the mechanism involved can be preferential vaporization of nickel in the weld pool.[12] Moreover, the formation of common intermetallics (Ni_3Ti, $NiTi_2$) can also alter the Ni to Ti ratio, which can dictate the intrinsic phase transformation temperatures.[14]

Modifications can also occur due to altered grain orientation and size of the solidification structure.[20,21] Although changes were not as substantial as those reported in the literature,[3,12] discrepancies may be attributed to the differences in thermomechanical history or process parameters used in previous studies.[4,9] Furthermore, it should not be forgotten that the aforementioned ways of adjusting phase transformations will also have a direct influence on the pseudoelastic properties.

IV. CONCLUSIONS

The current study analyzed the effects of Nd:YAG laser welding on the mechanical and phase transformation behaviors of crossed Nitinol wires. Joint formation was also studied *via* metallurgical observations. The key findings are as follows.

1. Removal of surface contaminants such as oxides is essential to laser welding of Nitinol. Entrapment of contaminants in the weld microstructure can significantly reduce the mechanical strength.
2. Welds in crossed Nitinol wires possessed excellent strength and were able to retain pseudoelasticity.
3. Fracture surfaces of base and weld metals revealed dimpled ductile surfaces. Failure mode was strongly dependent on the weld morphology. At low peak power inputs (below 0.8 kW), failure was initiated by welding defects. At the power range where maximum JBF was obtained (0.9 to 1.9 kW), failure occurred along the base and weld metals at lower powers and weld metal at higher powers.
4. The microstructure of crossed Nitinol wires consisted of columnar dendritic structure in the fusion zone and a recrystallized structure in the HAZ. Both fusion zone and HAZ grew with increased peak power inputs. Hardness reduced 30 pct in the fusion zone compared to the cold-worked base metal but was found to have little effect on the overall fracture strength.
5. Phase transformation behavior in the HAZ and fusion zone was altered, induced by the laser

Table II. Temperature Onsets of Phase Transformations in Welds Using Select Peak Powers

Peak Power	HAZ		Fusion Zone	
	M_s [K (°C)]	A_f [K (°C)]	M_s [K (°C)]	A_f [K (°C)]
0.6 kW	245.5 (−27.46)	269.5 (−3.49)	285.6 (12.57)	311.4 (38.44)
1.0 kW	248.9 (−24.12)	270.0 (−3.04)	280.7 (7.74)	307.2 (34.16)
1.6 kW	245.5 (−27.49)	269.2 (−3.81)	278.7 (5.68)	301.4 (28.36)

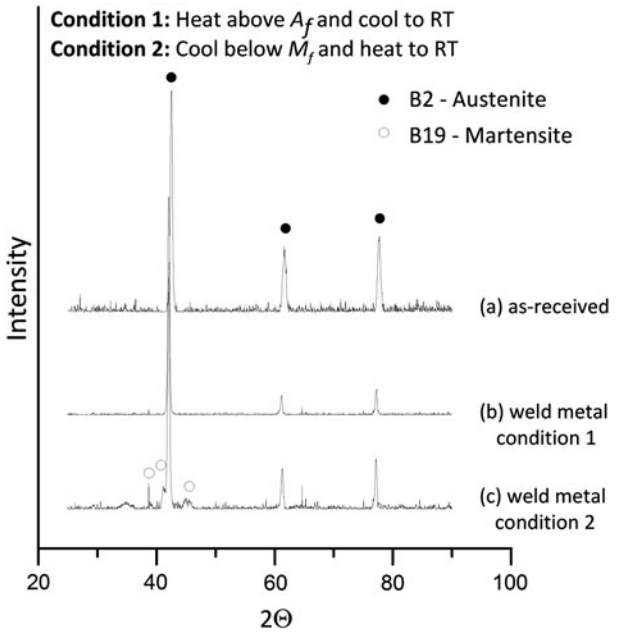

Fig. 17—Room-temperature XRD results for (*a*) as-received base metal and weld metal (1.0 kW) of (*b*) condition 1 and (*c*) condition 2.

welding process. The HAZ exhibited intrinsic phase transformation behavior due to the annealed structure that mimicked solution-treated Nitinol. The fusion zone showed phase transformations at higher temperatures, which could be thermally conditioned to have a structure of predominantly austenite or a mixture of martensite and austenite at room temperature.

ACKNOWLEDGMENTS

The authors acknowledge the support of the National Sciences and Engineering Research Council (NSERC) of Canada. The authors are also thankful to Mr. Dennis W. Norwich, Memry Corporation, for the kind donation of material examined in this study.

REFERENCES

1. J.V. Humbeeck: *Adv. Eng. Mater.*, 2001, vol. 3 (11), pp. 837–50.
2. X.J. Yan, D.Z. Yang, and X.P. Liu: *Mater. Charact.*, 2007, vol. 58, pp. 262–66.
3. X.J. Yan, D.Z. Yang, and M. Qi: *Mater. Charact.*, 2006, vol. 57, pp. 58–63.
4. Y. Zhou: *Microjoining and Nanojoining*, Woodhead Publishing Ltd, Cambridge, United Kingdom, 2008.
5. B. Tam: M.A.Sc Thesis, University of Waterloo, Waterloo, ON, Canada, 2010.
6. P. Scholossmacher, T. Haas, and A. Schüssler: *J. Phys. Coll. C5,* 1997, pp. 251–56.
7. Y. Ogata, M. Takatugu, T. Kunimasa, K. Uenishi, and K.F. Kobayashi: *Mater. Trans.*, 2004, vol. 45, pp. 1070–76.
8. Y.T. Hsu, Y.R. Wang, S.K. Wu, and C. Chen: *Metall. Mater. Trans. A*, 2001, vol. 32A, pp. 569–76.
9. A. Tuissi, S. Besseghini, T. Ranucci, F. Squatrito, and M. Pozzi: *Mater. Sci. Eng. A*, 1999, vols. A273–A275, pp. 813–17.
10. A. Falvo, F.M. Furgiuele, and C. Maletta: *Mater. Sci. Eng. A*, 2005, vol. 412, pp. 235–40.
11. Y.G. Song, W.S. Li, L. Li, and Y.F. Zheng: *Mater. Lett.*, 2008, vol. 62, pp. 2325–28.
12. M.I. Khan and Y. Zhou: *Mater. Sci. Eng. A*, 2010, vol. 527, pp. 6235–38.
13. X. Li, J. Xie, and Y. Zhou: *J. Mater. Sci.*, 2005, vol. 40, pp. 3437–43.
14. T.W. Duerig, K.N. Melton, D. Stockel, and C.M. Wayman: *Engineering Aspects of Shape Memory Alloys*, Butterworth-Heinemann, Oxford, United Kingdom, 1990.
15. G.S. Firstov, R.G. Vitchev, H. Kumar, B. Blanpain, and J. Van Humbeeck: *Biomaterials*, 2002, vol. 23 (24), pp. 4863–71.
16. V.G. Chuprina and I.M. Shalya: *Powder Metall. Met. Ceram.*, 2002, vol. 41 (1–2), pp. 85–89.
17. S.K. Sadrnezhaad and S.B. Raz: *Mater. Manuf. Process.*, 2008, vol. 23 (7), pp. 640–50.
18. B. Tam, M.I. Khan, and Y. Zhou: *MPMD 2009*, ASM International, Minneapolis, MN, 2009.
19. S. Kou: *Welding Metallurgy*, 2nd ed., John Wiley & Sons, Inc, Hoboken, NJ, 2002.
20. H. Sehitoglu, R. Hamilton, D. Canadinc, X.Y. Zhang, K. Gall, I. Karaman, Y. Chumlyakov, and J.J. Maier: *Metall. Mater. Trans. A*, 2003, vol. 34A, pp. 5–13.
21. F.J. Gil, J.M. Manero, and J.A. Planell: *J. Mater. Sci.*, 1995, vol. 30, pp. 2526–30.